Structure of the *Rhodobacter sphaeroides* Light-Harvesting 1 β Subunit in Detergent Micelles[†,‡]

Paul L. Sorgen,[§] Sean M. Cahill,[§] Ray D. Krueger-Koplin,[§] Suzanne T. Krueger-Koplin,[§] Craig C. Schenck,[||] and Mark E. Girvin*[,§]

Department of Biochemistry, Albert Einstein College of Medicine, Bronx, New York 10461, and Department of Biochemistry and Molecular Biology, Colorado State University, Fort Collins, Colorado 80523

Received July 30, 2001; Revised Manuscript Received October 30, 2001

ABSTRACT: The light harvesting 1 antenna (LH1) complex from *Rhodobacter sphaeroides* funnels excitation energy to the photosynthetic reaction center. Our ultimate goal is to build up the structure of LH1 from structures of its individual subunits, much as the antenna can self-assemble from its components in membrane-mimicking detergent micelles. The β subunit adopts a nativelike conformation in Zwittergent 3:12 micelles as demonstrated by its ability to take the first step of assembly, binding BChl *a*. Multidimensional NMR spectroscopy shows that the β subunit folds as a helix$_{(L12-S25)}$−hinge$_{(G26-W28)}$−helix$_{(L29-W44)}$ structure with the helical regions for the 10 lowest-energy structures having backbone rmsds of 0.26 and 0.24 Å, respectively. Mn^{2+} relaxation data and the protein−detergent NOE pattern show the C-terminal helix embedded in the micelle and the N-terminal helix lying along the detergent micelle surface with a 60° angle between their long axes. ^{15}N relaxation data for residues L12−W44 are typical of a well-ordered protein with a correlation time of 8.25 ± 2.1 ns. The presence of the hinge region placing the N-terminal helix along the membrane surface may be the structural feature responsible for the functional differences observed between the LH1 and LH2 β subunits.

The conversion of light energy to chemical energy in bacterial photosynthesis proceeds through a series of specialized membrane-spanning protein−pigment complexes. The initial stage involves the light-harvesting complexes (LH1 and LH2)[1] and the reaction center (RC). Light absorbed by the LH1 and LH2 carotenoid and bacteriochlorophyll *a* (BChl *a*) molecules is transferred as excitation energy to the RC. The excitation induces a charge separation from the excited primary donor, a BChl *a* dimer called the special pair, which accumulates at the quinone (Q_B) site. A doubly reduced quinone accepts protons (Q_BH_2) from the cytoplasm and then is released from the RC to diffuse to the cytochrome bc_1 complex. The cytochrome bc_1 complex catalyzes the oxidation of the quinone to release protons into the periplasmic space. The proton gradient created by this process is used by the ATP synthase, which completes the conversion of light energy to chemical energy.

Detailed structures of the LH2, RC, and cytochrome bc_1 complexes (*1*−*5*) have greatly enhanced the understanding of bacterial photosynthesis. However, no high-resolution structure of LH1 currently exists. A projection map at 0.85 nm resolution of the LH1 complex from *Rhodospirillum rubum* obtained by cryoelectron microscopy showed an arrangement of 16 identical subcomplexes positioned in a ringlike structure (*6*). One subcomplex of LH1 consists of an $\alpha\beta$ heterodimer (58 and 48 amino acids, respectively) binding two molecules of BChl *a* and one carotenoid (*7*−*10*). RC−LH1 two-dimensional crystals placed the RC within the ring of LH1 (*11*, *12*). A molecular model for the *Rhodobacter sphaeroides* LH1 based upon its close homology to LH2 also supports a hexadecamer structure (*13*, *14*). Recently, a structure of the *Rb. sphaeroides* β subunit in organic solvents was determined, illustrating two helical regions separated by a more flexible linker (*15*).

Although a structural determination of the LH1 complex (>200 kDa) is beyond current NMR techniques, the symmetry observed for LH1 can be exploited to simplify the study of its structure. If the structure of a dissociated subunit or subcomplex accurately represents the structure of a fully associated subunit, then the LH1 structure can be determined by the sum of its parts. By adjustment of the ratios of detergent, subunits, and BChl *a*, discrete stable complexes can be formed ranging from individual α and β subunits, through the B777 (1BChl *a* with 1α or 1β) and B820 ($\alpha\beta$-2BChl *a* or β_2-2BChl *a*) subcomplexes, to the full LH1 complex (B870) (*16*, *17*). Determining the structures of individual subunits and subcomplexes in a membrane environment provides a foundation for determining the LH1 structure, and will provide the first structural details on what,

[†] This work was supported by U.S. Public Health Service Grants GM58171 and F32 GM20504.

[‡] Coordinates have been deposited in the Protein Data Bank (entry 1JO5).

* To whom correspondence should be addressed: Department of Biochemistry, Albert Einstein College of Medicine, Bronx, NY 10461. Fax: (718) 430-8565. E-mail: girvin@aecom.yu.edu.

[§] Albert Einstein College of Medicine.

[||] Colorado State University.

[1] Abbreviations: $^3J_{HN\alpha}$, three-bond H^N-H^α coupling constants; β-OG, *n*-octyl β-D-glucopyranoside; BChl *a*, bacteriochlorophyll *a*; DPC, dodecylphosphocholine; HSQC, heteronuclear single-quantum correlation; LH, light-harvesting; MPG, myristoyllysophosphatidylglycerol; NMR, nuclear magnetic resonance; NOE, nuclear Overhauser effect; NOESY, NOE spectroscopy; RC, reaction center; rmsd, root-mean-square deviation; SDS, sodium *n*-dodecyl sulfate.

10.1021/bi011576j CCC: $22.00
Published on Web 12/11/2001

if any, conformational changes take place during the assembly process of a large membrane protein complex.

We have used multidimensional NMR to determine the solution structure of the β subunit from *Rb. sphaeroides* LH1 in Zwittergent 3:12 micelles as a mimetic for native membranes. We have found detergent solution conditions in which high-resolution NMR data can be obtained, and in which the β subunit binds BChl *a* to form B820 (β_2-2BChl *a*). The β subunit folds as a helix−hinge−helix structure. A model is presented to illustrate the position of the β subunit in a Zwittergent 3:12 micelle.

EXPERIMENTAL PROCEDURES

Sample Preparation. The LH1 β subunit was overexpressed from a genomic deletion strain of *Rb. sphaeroides* (SK102). SK102 was modified to eliminate genomic expression of the LH2 peptides, the L and M subunits of the RC, and pufX. SK102 was grown in the dark at 34 °C using 1.8 L of M22 minimal medium in a 2 L flask with cotton plugging the neck to limit the O_2 concentration. Uniform ^{15}N and/or ^{13}C labeling was achieved by growing cells with 1.5 mM $(^{15}NH_4)_2SO_4$ and 11.1 mM [^{13}C]glucose as the sole nitrogen and carbon sources, respectively. Deuterium was incorporated by cell growth in 100% D_2O. SK102 was acclimated to D_2O by increasing the D_2O/H_2O ratio in 20% increments starting with 20%.

Chromatophores were prepared from cells suspended in water and disrupted by two passages through a French pressure cell at 20 000 psi. Cell debris was removed by centrifugation (Sorvall GSA rotor, 12 000 rpm, 15 min), and the chromatophores were collected by high-speed centrifugation (Beckman Ti-45 rotor, 45 000 rpm, 1.5 h) and lyophilized to dryness. The β subunit was extracted from 1.2 g of dried chromatophores by 3 × 10 mL organic solvent washes [1/1 $CHCl_3$/MeOH mixture and 100 mM ammonium acetate (pH 7.5)] (*18*). The extract was chromatographed on a LH60 column (120 cm × 4.8 cm), and fractions containing the β subunit were dialyzed in spectra/Por 1 membranes (molecular mass cutoff of 6−8 kDa) against water at 4 °C for 60 h. The precipitated β subunit at the interface between the water and remaining chloroform was collected, frozen at −80 °C, lyophilized to dryness, and stored at −20 °C.

NMR samples (1.7 mM) of the purified uniformly isotopically labeled (^{15}N, ^{15}N and ^{13}C, or ^{2}D, ^{15}N, and ^{13}C) β subunit were prepared in 300 μL (95% H_2O/5% D_2O) of 8% Zwittergent 3:12 and 50 mM phosphate buffer (pH 6.5). Sample stability was monitored by ^1H and $^1H-^{15}N$ HSQC spectra before and after each three-dimensional (3D) NMR experiment. The half-life of each sample was approximately 1 week.

BChl a Purification. BChl *a* was extracted from chromatophores of a *Rb. sphaeroides* deletion strain WS231BG, lacking carotenoids, by 3 × 30 mL methanol extractions. The methanol used to extract BChl *a* from the chromatophores was evaporated to give a final BChl *a* concentration of approximately 1 mg/mL. Aliquots (400 μL) were loaded onto a Waters Radial-Pac C18 reverse-phase HPLC column (8 mm × 200 mm), and BChl *a* was eluted isocratically with methanol at 1.8 mL/min. The BChl *a* concentration was calculated using an ϵ_{770} of 63 500 M^{-1} cm^{-1} (*19*). Methanol was removed by evaporation under argon, and dried BChl *a* was stored in the dark at −20 °C.

NMR Spectroscopy. NMR data were acquired at 37 °C using a Bruker DRX-600 spectrometer fitted with a triple-resonance probe and triple-axis gradients. All experiments made use of pulsed field gradients for coherence selection and artifact suppression (*20*, *21*). Sensitivity enhancement schemes (*21*, *22*) were used in the pulse programs wherever possible. Quadrature detection in the indirect dimensions was via States−TPPI, TPPI, or States depending on the individual experiments (*23*). ^1H chemical shifts were referenced directly to TSP [3-(trimethylsilyl)propionic acid] at 0 ppm, and ^{15}N and ^{13}C were referenced indirectly (*24*). NMR spectra were processed using NMRPipe (*25*). The data in all indirect dimensions were extended by linear prediction and zero filling. Data were analyzed using NMRView (*26*).

Backbone sequential assignments were obtained using the following 3D experiments: HNCACB (*27*), CBCA(CO)NH (*28*), HNCA (*29*), HNCO (*30*), HN(CO)CA (*31*), HNHA (*32*), and HCACO (*33*). Side chain chemical shifts were obtained from 3D HCCH-TOCSY (*34*) and ^{15}N TOCSY-HSQC (*35*) experiments. Distance constraints were derived from NOEs observed in ^{15}N NOESY-HSQC and ^{13}C NOESY-HSQC (*35*) spectra, with mixing times of 125 and 150 ms, respectively.

Backbone Hydrogen Bonds. Hydrogen bonds were identified on the basis of slowly exchanging backbone amide protons (*36*) and temperature dependence studies (*37*). For the amide proton−deuterium exchange experiment, the β subunit was initially solubilzed in detergent solution to allow insertion of the membrane-spanning region into the micelle. The sample was then diluted to a final D_2O concentration of 60%. A series of 4 h ^{15}N HSQC spectra were recorded over a 3 day period, and amide proton signals with half-lives of exchange greater than 1 day were considered likely to be hydrogen-bonded. The side chain glutamines were used as an internal control for fast exchange to follow the loss of signal unrelated to hydrogen−deuterium exchange (i.e., aggregation or precipitation). Temperature dependence studies followed the amide proton chemical shifts from 12 to 37 °C. Any amide proton that shifted less than 4.5 ppb/K was considered likely to be hydrogen-bonded. The data from these two experiments were compared, and an amide proton hydrogen bonding constraint was imposed only if it appeared to be hydrogen-bonded by both criteria. Each hydrogen bond was imposed as two distance restraints (H−O distance of 1.9−2.3 Å and N−O distance of 2.4−3.0 Å).

^{15}N Relaxation Experiments. The pulse sequences used for measuring ^{15}N T_1 and T_2 relaxation times and $^{15}N\{^1H\}$ NOEs are described by Skelton et al. (*38*) and were modified to include watergate-based water suppression (*39*) as described by Fushman et al. (*40*). The NOE experiment was also modified to reduce the extent of magnetization exchange between the amide protons and water protons according to Grzesiek and Bax (*41*). Data sets for the T_1 and T_2 experiments were collected with 4K and 192 complex points in F_2 (^1H) and F_1 (^{15}N), respectively, with 32 scans per t_1 point and a recycle delay of 1 s. Data sets for the NOE experiments were collected with 2K and 64 complex points in F_2 (^1H) and F_1 (^{15}N) respectively, with 96 scans per t_1 point and a recycle delay of 6 s. All experiments used a proton sweep width of 7800 Hz and a ^{15}N sweep width of 2500 Hz with the ^1H and ^{15}N carriers set to 4.7 and 119 ppm, respectively.

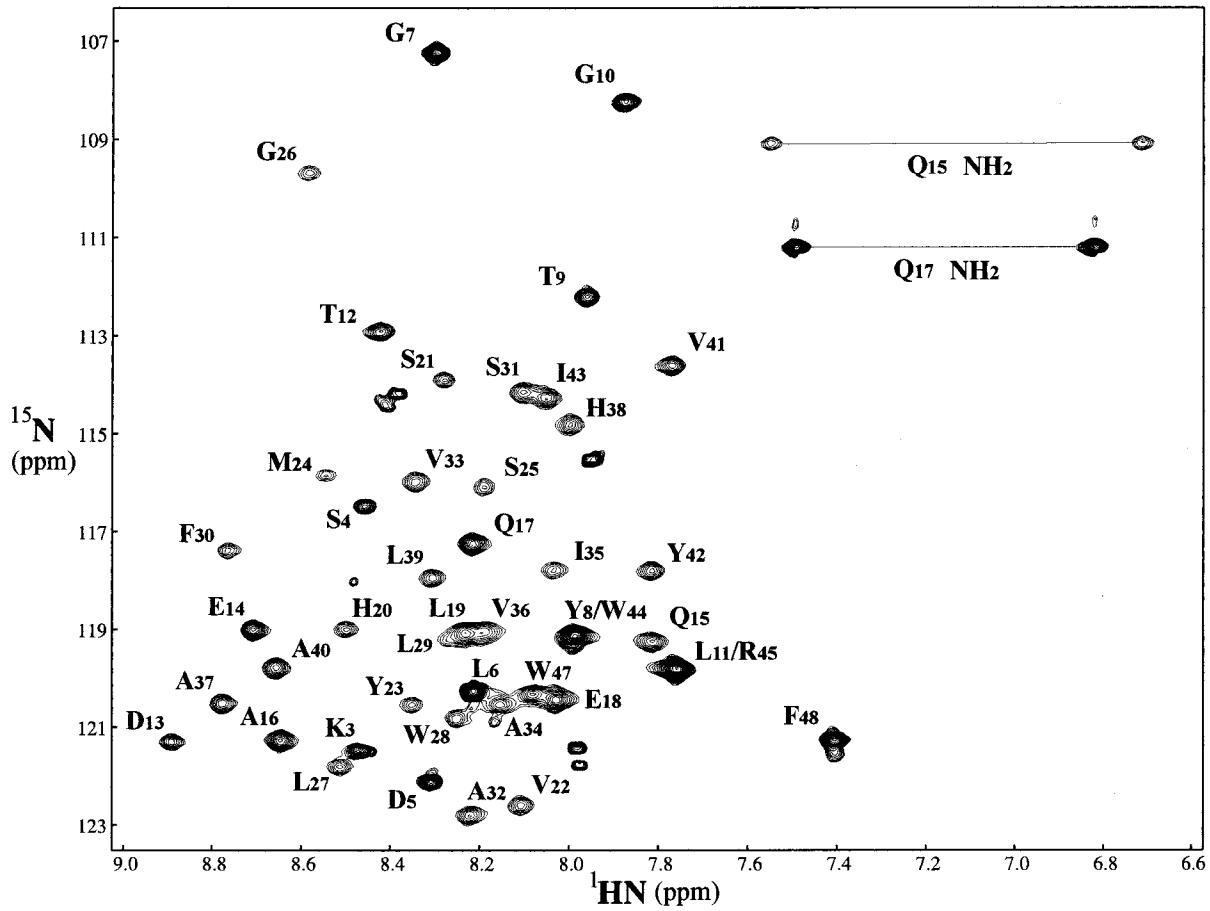

FIGURE 1: $^{1}H-^{15}N$ HSQC spectrum of the *Rb. sphaerodies* LH1 β subunit in detergent micelles. The spectrum was recorded using 1.7 mM β subunit dissolved in 50 mM phosphate buffer (pH 6.5) and 8% Zwittergent 3:12 at 37 °C. Amide cross-peaks are labeled.

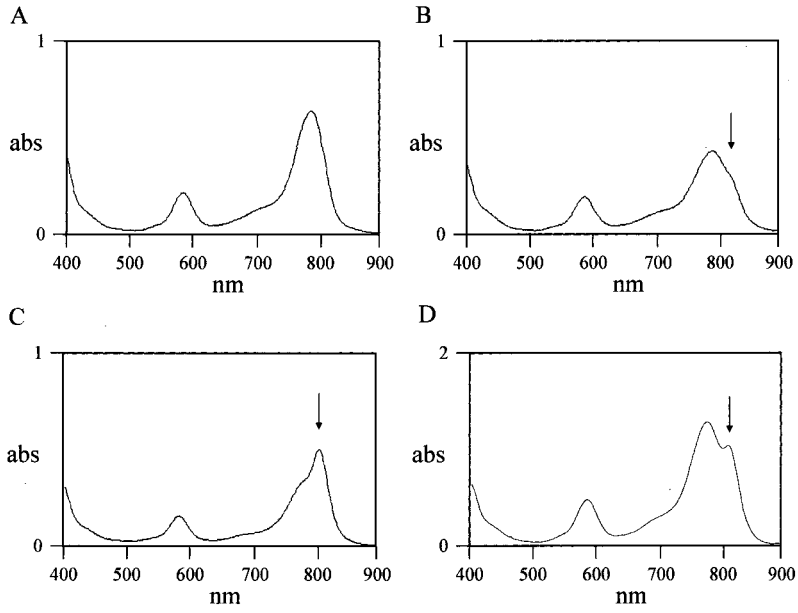

FIGURE 2: Binding of bacteriochlorophyll *a* (BChl *a*) to the LH1 β subunit in Zwittergent 3:12 micelles. (A) No subcomplex formation: B774 (1 mM BChl *a* and 1 mM β subunit in 1% Zwittergent 3:12 at 25 °C). (B) Initial B820 subcomplex formation (0.13 mM BChl *a* and 0.13 mM β subunit in 0.13% Zwittergent 3:12 at 25 °C). (C) B820 subcomplex formation (0.031 mM BChl *a* and 0.031 mM β subunit in 0.031% Zwittergent 3:12 at 25 °C). (D) Initial B820 subcomplex formation under NMR conditions (2.8 mM BChl *a* and 2.4 mM β subunit in 1.83% Zwittergent 3:12 at 32 °C). Arrows indicate B820 formation.

The T_2 measurements were performed with transverse relaxation delays of 8, 16 (twice), 24, 32, 40, 48, 64 (twice), 128, 160, 240 (twice), and 320 ms, and a 1 ms delay was used between ^{15}N pulses in the Carr−Purcell−Meiboom−Gill sequence during the transverse relaxation period. The T_1 measurements were performed with longitudinal relaxation delays of 8, 20 (twice), 40, 100 (twice), 160, 200, 300 (twice), 500, and 800 ms and 2 and 4 s. $^{15}N\{^{1}H\}$ steady-

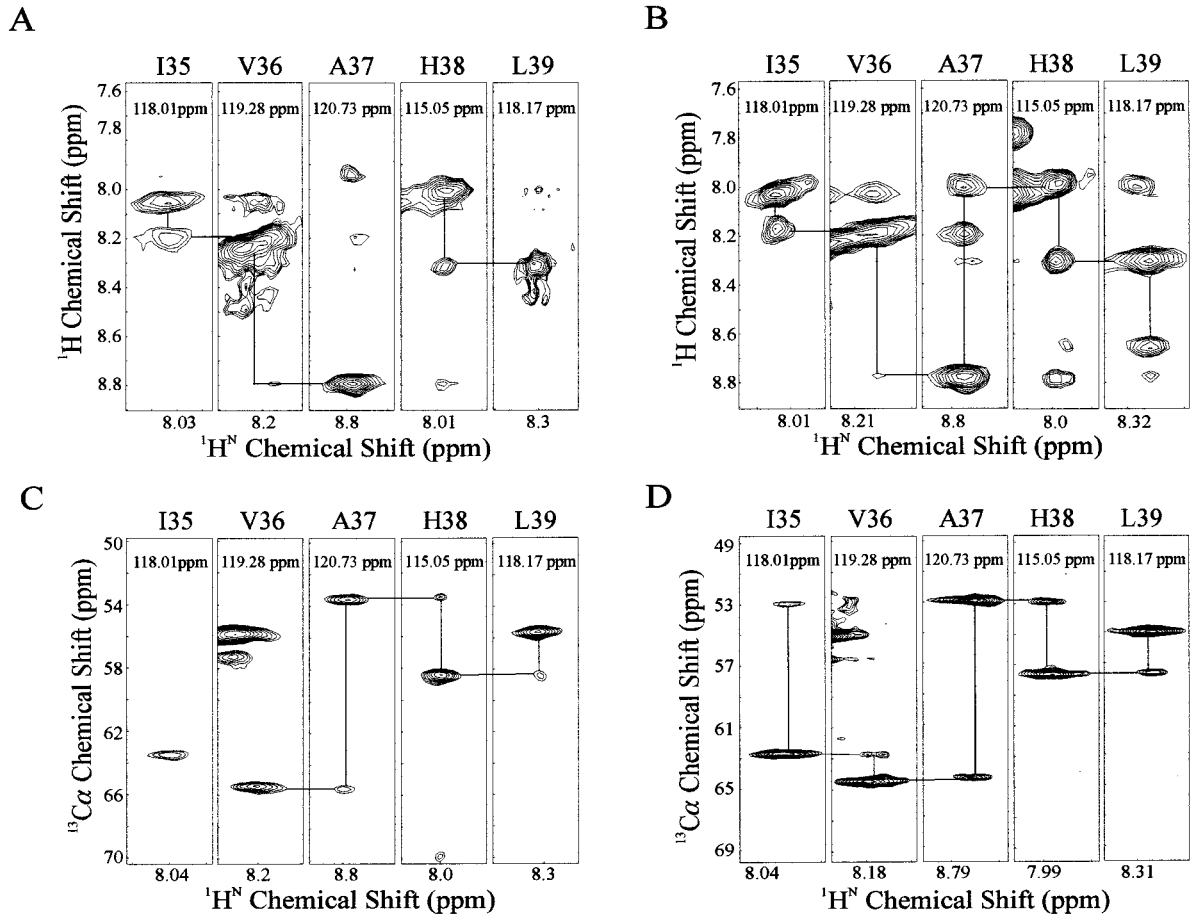

FIGURE 3: Example assignment strips from two inter-residue 3D experiments demonstrating the enhanced resolution and signal to noise from a deuterated β subunit. Sequential strips for membrane-spanning residues I35−L39 from (A) ^{15}N NOESY-HSQC, (B) ^{2}D-decoupled ^{15}N HSQC-NOESY, (C) HNCA, and (D) ^{2}D-decoupled HNCA data sets. Strips from the NOESY experiments were taken at the intraresidue diagonal peak to show all inter-residue cross-peaks. Lines illustrate the sequential connections when possible. The ^{15}N chemical shift is listed in each panel.

state NOE values were obtained by recording spectra with and without a 3 s GARP proton decoupling period applied in the middle of the amide spectral region during the recycle delay. Relaxation data were analyzed using the program Dasha (*42*).

Structure Calculation. Model structures were calculated by simulated annealing using torsion angle dynamics as implemented in the program CNS (*43*). NOE cross-peaks classified as strong, medium, and weak were converted into distance restraints of 1.8−2.5, 1.8−3.5, and 1.8−5.5 Å, respectively. Torsion angle restraints were obtained from chemical shift analysis using the TALOS program (*44*). $^3J_{HN\alpha}$ coupling constants were measured from a 3D HNHA experiment (*32*), and used directly as constraints. The 10 best minimized structures were evaluated using AQUA and PROCHECK-NMR (*45*).

RESULTS

Sample Conditions. Sample conditions were optimized to obtain high-resolution spectra of the β subunit in detergent micelles for structural determination. Initial samples made in the *n*-octyl β-D-glucopyranoside (β-OG) detergent [1 mM β subunit in 4.5% β-OG and 50 mM phosphate (pH 7.5)], as used in many LH1 studies for purification and characterization of the complex (*46*−*49*), had a half-life of only 1 day and poor dispersion in a ^{15}N HSQC spectrum (data not shown). To optimize sample conditions, we investigated numerous detergents [Zwittergent 3:8, 3:10, 3:12, and 3:14 (*50*), *n*-dodecyl β-D-maltoside (DM), dodecylphosphocholine (DPC), 3-[(cholamidopropyl)dimethylammonio]-1-propanesulfonate (CHAPS), lauryldimethylamine oxide (LDAO), and sodium *n*-dodecyl sulfate (SDS)], detergent concentrations (1−8%), temperatures (25−55 °C), protein concentrations (1−5 mM), salt concentrations (50−250 mM phosphate buffer), and pHs (6.5−7.5) (data not shown). The optimal sample conditions were found to be 1.7 mM β subunit in 8% Zwittergent 3:12 and 50 mM phosphate buffer at pH 6.5 and 37 °C (Figure 1). The half-life of the β subunit under these conditions was approximately 1 week. The single most important factor was the detergent. The β subunit was not stable in detergents with sugar headgroups, net charges, or small chain lengths, as indicated by half-lives of <1 day. The half-life of the β subunit was extended by increasing the detergent concentrations up to 4%. Even though there was no increase in stability between 4 and 8%, the higher concentration was used to obtain a more homogeneous population of micelles containing a single β subunit. Temperature and pH affected resolution in the ^{15}N HSQC spectrum. The β subunit in Zwittergent 3:12 was stable up to 45 °C, but above this temperature, an irreversible loss of signal occurred. The maximum stable protein concentration was 1.7 mM. In samples prepared at up to 5 mM β subunit,

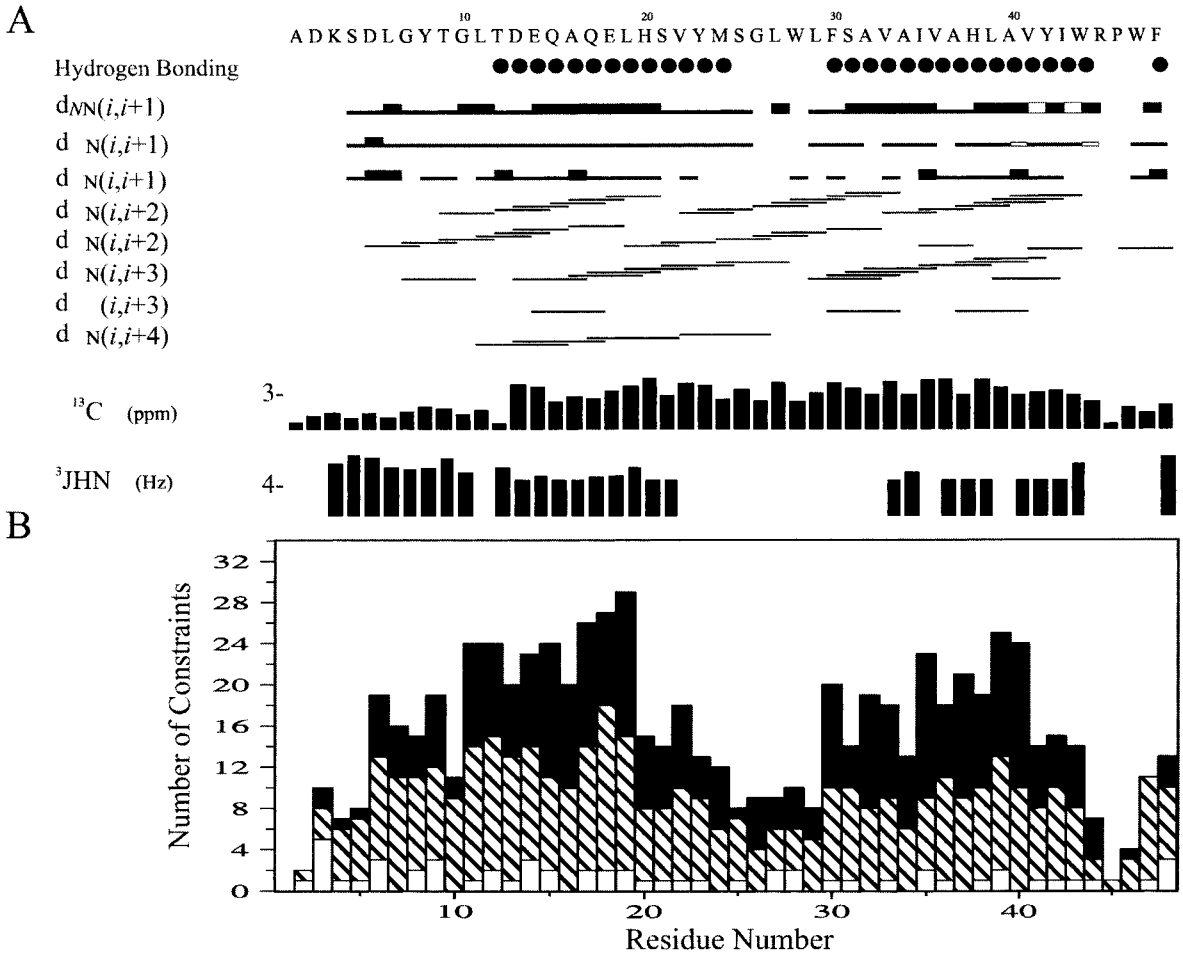

FIGURE 4: Summary of NMR restraints derived for the LH1 β subunit. (A) Black circles indicate hydrogen bonding determined from hydrogen−deuterium exchange and variable-temperature experiments. Horizontal lines identify backbone NOEs with the thickness indicating approximate cross-peak intensity. $^3J_{HN\alpha}$ and $^{13}C\alpha$ chemical shift deviations from random coil values are also shown. (B) Number of NOE restraints per residue. White bars indicate intraresidue NOEs; hatched bars indicate $i-i+1$ sequential NOEs, and black bars indicate medium-range NOEs.

the signal intensities decayed to the level observed in the 1.7 mM sample over the course of 24 h, but then remained at that level with the typical half-life of 1 week.

B820 Subcomplex Formation. A major concern for any protein under new sample conditions is its biological activity. To test if the β subunit was properly folded in Zwittergent 3:12 micelles, we investigated its ability to bind BChl *a* and form nativelike higher subcomplexes (Figure 2). The binding of BChl *a* to the β subunit can be followed optically by the red shifting of the Q_y band from unbound BChl *a* at 774 nm through β_2-2BChl *a* formation at 820 nm (*46*). Our initial test was to see whether subcomplex formation could occur in Zwittergent 3:12 detergent. Controls for this experiment showed that the β subunit alone has no absorbance at 774 nm and BChl *a* alone has one Q_y absorbance peak at 774 nm (data not shown). The β subunit and BChl *a* were combined at a high detergent concentration which prevents binding (Figure 2A). As the detergent concentration is decreased by the addition of buffer alone [50 mM phosphate buffer (pH 6.5)], B820 formation occurs (Figure 2B,C). B820 can also be formed at the concentrations and temperature needed for NMR (Figure 2D). The absorbance data demonstrate that the β subunit retains its native ability to bind BChl *a* and form larger complexes in Zwittergent 3:12.

Resonance Assignments. The triple-resonance spectra allowed identification and sequential assignment of all backbone amide resonances (Figure 1). Consistently, the weakest signals observed in all NMR experiments belonged to what appears to be a hinge region (G26−W28), while the strongest signals and best resolution came from the N-terminal residues. A larger number of experiments was required to make the assignments for the β subunit than typically would be used for proteins of this size. All ^{13}CO and $^{13}C^{\alpha}$ resonances were assigned, and most of $^{13}C^{\beta}$ resonances were found with the exception of those from L29, W44, and R45. All protonated ^{15}N resonances for the glutamine, tryptophan, and arginine side chains were also assigned.

Except for the HNCO, no single triple-resonance experiment gave more than 85% of the expected cross-peaks with a ^{15}N- and ^{13}C-labeled protein. The cross-peaks consistently missing were from the hinge region (G26−W28) and the C-terminus (W44−P46). To identify the missing resonances, we resorted to a ^2D-, ^{15}N-, and ^{13}C-labeled β subunit. The replacement of ^1H with ^2D increased sensitivity in a HNCA experiment and the amide−amide region of a 3D ^2D-decoupled ^{15}N NOESY-HSQC experiment by removing contributions to proton line widths from proton−proton dipolar relaxation and $^1H-^1H$ scalar couplings. Figure 3 illustrates the signal enhancement from deuterium-labeled protein by comparing slices for protonated and deuterated samples in the 3D ^{15}N NOESY-HSQC (Figure 3A) and ^2D-

decoupled ^{15}N NOESY-HSQC spectra (Figure 3B) and the 3D HNCA (Figure 3C) and ^{2}D-decoupled HNCA spectra (Figure 3D). Additional peaks were identified in the HNCA and ^{2}D-decoupled ^{15}N NOESY-HSQC spectra with the deuterium-labeled β subunit. With deuteration, all expected cross-peaks were present in the HNCA and 20 more amide−amide connections were identified in the ^{15}N NOESY-HSQC spectra. The deuterium labeling also decreased the potential for misassignment by decreasing the $^{13}C^{\alpha}$ line widths from 150 to 15 Hz. Full assignments have been deposited at the BMRB (accession number 4949).

Constraints for Structural Calculations. NOEs from all protons to the amide protons were identified in a 3D ^{15}N NOESY-HSQC spectrum and a 3D ^{2}D-decoupled ^{15}N NOESY-HSQC spectrum. Figure 4A summarizes the backbone NOEs observed for the β subunit. Nearly all of the 219 amide NOEs observed were characteristic of an α helix. From the amide NOE patterns alone, the protein appeared to be helical from T12 through S25 and from L29 through W44. No long-range NOEs were detected. Secondary $^{13}C^{\alpha}$ chemical shifts (*51*) were also consistent with these segments of helical secondary structure (Figure 4A). The 3D ^{13}C NOESY-HSQC spectra provided 54 proton to carbon proton NOEs. Few NOEs were observed from the aromatic side chains. Altogether, 37 restraints were intraresidue, 143 were short-range, and 93 were medium-range. The total number of NOE constraints observed per residue is illustrated in Figure 4B. The reduced number of inter-residue NOEs observed between G26 and W28 (approximately seven each) is consistent with a break in structure between the two helical regions. No additional amide−amide NOEs for G26−W28 were observed in the deuterium-labeled β subunit. A total of 28 $^{3}J_{HN\alpha}$ coupling constants were measured from the HNHA experiment (*32*). The $^{3}J_{HN\alpha}$ data indicated an unstructured N-terminus (A1−L11), followed by a predominately helical structure. Both hydrogen−deuterium exchange and amide temperature coefficients identified two segments of stable hydrogen-bonded secondary structure: residues T12−M24 and F30−W44. Hydrogen bonding restraints were added for these residues. The hydrogen bonding data, carbon chemical shifts, and NOE data are consistent with a break between the hydrophilic and hydrophobic helical regions

Structure Calculation and Description. Structure calculations by torsion angle dynamics followed with refinement by simulated annealing and energy minimization led to the family of structures shown in Figure 5A. The structures were superimposed on the basis of the backbone coordinates from T12−W44, which includes a somewhat less well-defined hinge region (G26−W28) between the two helical segments. The total rmsd for this alignment was 1.58 Å. The main difference between these structures was due to the rotation of the N-terminus on the surface of the micelle relative to the C-terminal helix caused by variations in this hinge region. The structural models fit the NMR data well, with no violations of experimental distance restraints greater than 0.35 Å. The positions of the backbone and most side chain atoms were well-defined by the NMR restraints. This becomes clearer when the hydrophilic region between T12 and S25 (Figure 5B), the membrane-spanning region between L29 and W44 (Figure 5C), and the hinge region of G26−W28 are aligned separately. The rmsds for the hydrophilic, membrane-spanning, and hinge regions are 0.26, 0.24, and 0.60 Å, respectively. Structural statistics are presented in Table 1.

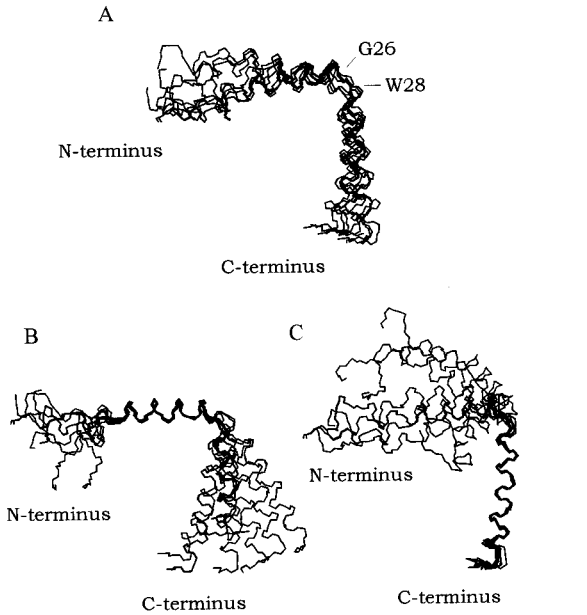

FIGURE 5: Solution structure of the LH1 β subunit in detergent micelles. Backbone traces of the 10 LH1 β subunit NMR conformers that best represent the structure are aligned by superimposing the backbone atoms of residues (A) 12−44, (B) 12−25, and (C) 30−44. All images were produced using MOLMOL (*73*).

Table 1: Structural Statistics of the 10 LH1 β Subunit Structures

no. of NOE distance restraints (total of 273)	
intraresidue	37
sequential	143
medium-range	93
long-range (interhelix)	0
no. of backbone hydrogen bonds	29
rmsd of atomic coordinates	
(residues 12−25, 29−44, and 26−28)	
backbone (Å)	0.26, 0.24, 0.60
all non-hydrogens (Å)	1.14, 1.08, 1.21
deviations from experimental distance restraints	
largest (Å)	0.35
rmsd (Å)	0.036
Ramachandran plot	
residues in most favored regions	92.1%
residues in additional allowed regions	6.7%
rmsd from ideal geometry	
bond lengths (Å)	0.0023
bond angles (deg)	0.429
impropers (deg)	0.251

The overall structure of the β subunit in detergent micelles is two helical sections separated by a hinge region. The C-terminal helix (L29−W44) is inserted in the detergent micelle, as evidenced by the 12 strong NOEs (<3.5 Å distances) observed between the backbone amides in the membrane-spanning region and the aliphatic protons of the Zwittergent 3:12 detergent (Figure 6A,C). The C-terminal residues (R45−F48) fold back toward the membrane-spanning helix. The N-terminus is highly flexible and mostly unstructured (A1−L11), although six of the 10 calculated structures have helical tendencies. The N-terminal helix extends from T12 through S25. Some residues in the N-terminal helix show weak NOEs (<5.5 Å distances) to the aliphatic protons of the Zwittergent 3:12 detergent (Figure 6A,C). The pattern of N-terminal helix NOEs to detergent has a helical periodicity, with residues Q17, S21, and M24

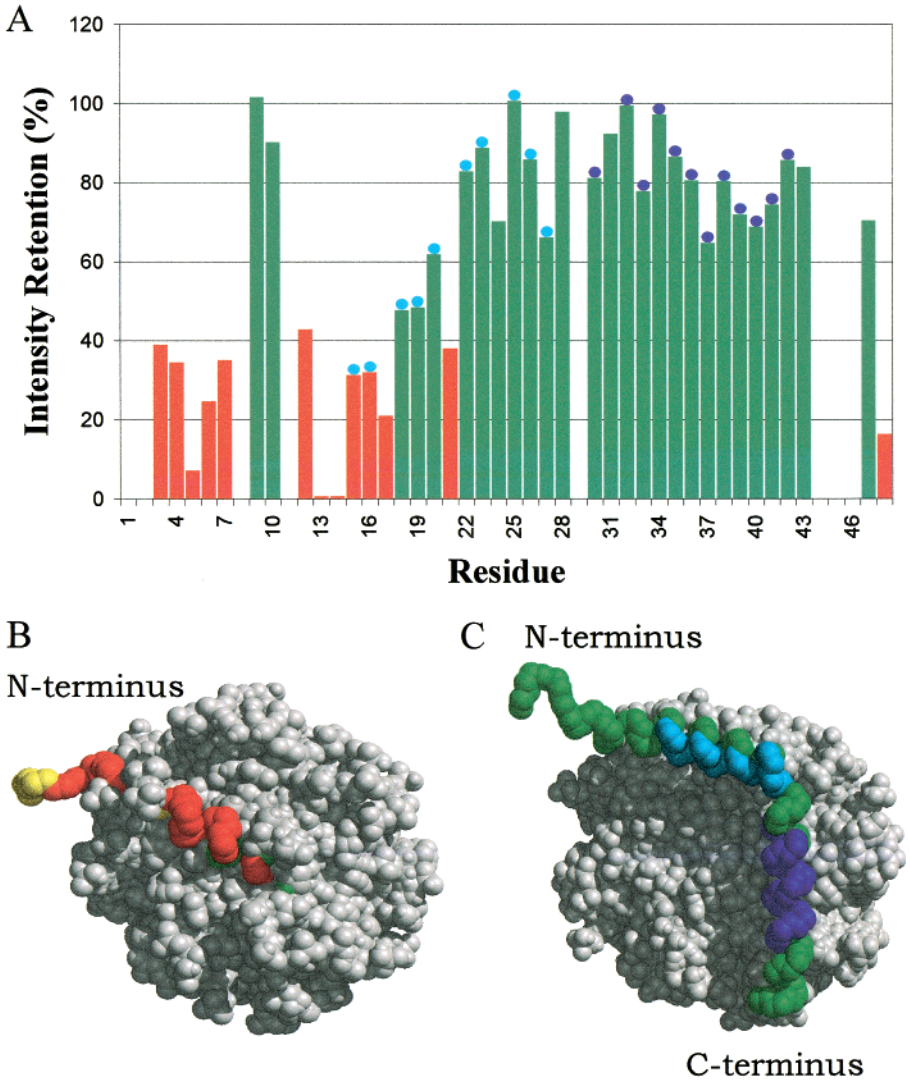

FIGURE 6: Positioning of the LH1 β subunit in a Zwittergent 3:12 micelle modeled from Mn^{2+} and NOE data. (A) Ratio of ^{15}N HSQC peak intensities from the LH1 β subunit in the presence and absence of 1 mM Mn^{2+}. Green bars and red bars denote protected and solvent-exposed amino acids, respectively. Dark blue circles denote residues with strong NOEs to the aliphatic region of the detergent, and light blue circles denote residues with weak NOEs. (B) Top view of the LH1 β subunit in a Zwittergent 3:12 micelle. Colors correspond to the bars in panel A. Yellow indicates residues not resolved in the Mn^{2+} experiment. (C) Side view of a β subunit in a Zwittergent 3:12 micelle with half the micelle removed, which is modeled to correspond with the detergent NOE data. The dark and light blue colors correspond to the circles in panel A. Green denotes residues with no detergent NOEs. A model of Zwittergent 3:12 was created in Alchemy III (Tripos Inc.), and the models were created in MidasPlus (*74*, *75*).

exhibiting no detergent NOE cross-peaks. The approximate 60° angle between the N- and C-helices is consistent with contact of the N-terminal helix with the detergent micelle, and the pattern of NOE peaks to the Zwittergent 3:12 suggests that one face of the N-terminal helix lies embedded in the Zwittergent 3:12 micelle.

To confirm that one face of the N-terminal helix is embedded in the micelle, we added the paramagnetic species Mn^{2+}, and looked for line broadening of solvent-exposed residues in a ^{15}N HSQC spectrum. $MnCl_2$ was added to 1.7 mM β subunit at increasing concentrations (0.01, 0.1, 1, and 5 mM). Data for the 1 mM $MnCl_2$ experiment are illustrated in Figure 6A. The membrane-spanning region was unaffected as expected, because Mn^{2+} does not enter the membrane. The N-terminus is solvent-exposed, based on the reduced cross-peak intensity. Residues D13 and E14 lost all signal in the presence of Mn^{2+}, which can be explained by a combination of being solvent-exposed and their negatively charged side chains binding Mn^{2+}. More importantly, the Mn^{2+} affected the hydrophilic N-terminal helix in an amphipathic manner as modeled in Figure 6B. Furthermore, the β subunit probably associates with the membrane as early as T9, as indicated by complete protection against Mn^{2+}. Combining the structural, Mn^{2+} relaxation, and detergent NOE data, we find residues Q17, S21, and M24 face the solvent side with Q17 and S21 completely solvent exposed. These experiments provide evidence that one face of the hydrophilic N-terminal helix lies embedded in the Zwittergent 3:12 micelle, implying that the hinge region is a necessary structural feature, and not just an artifact from the limited number of NOEs. These results could not be explained if the N-terminal helix extended straight out of the Zwittergent 3:12 micelle and was fully solvent exposed.

^{15}N Relaxation. ^{15}N relaxation measurements were performed to characterize the overall motion of the β subunit backbone in detergent micelles. The T_1, T_2, and $^{15}N\{^1H\}$

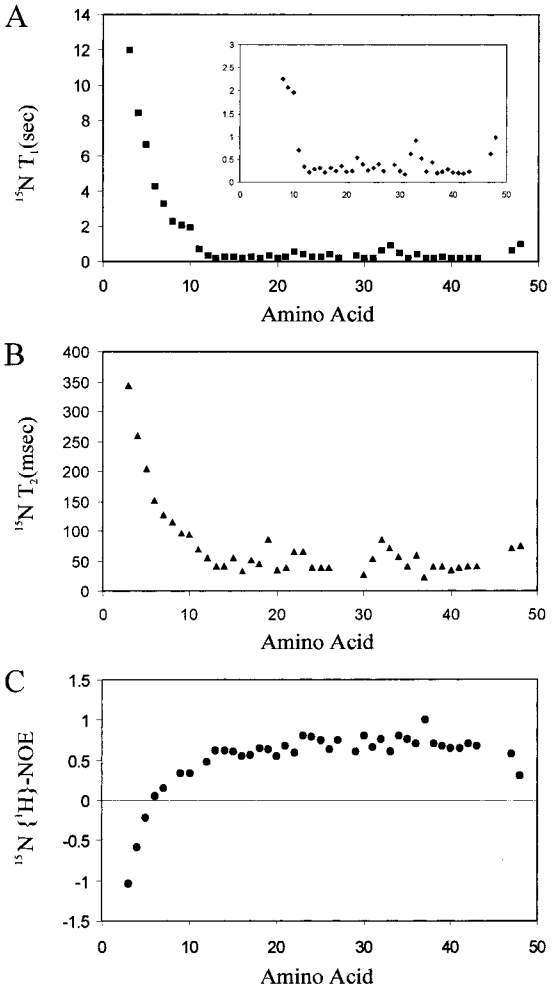

FIGURE 7: Relaxation measurements of the LH1 β subunit in detergent micelles. Plots of ^{15}N (A) T_1, (B) T_2, and (C) NOE values as a function of residue number.

NOE results are shown in Figure 7A−C. The relaxation values are consistent with a highly dynamic N-terminus (A1−L11). The remainder of the β subunit behaves as a more rigid body. The long T_1 and T_2 values for the N-terminus are typical of disordered polypeptides, while those for residues T12−W47 are typical of a well-ordered protein with an overall correlation time of 8.25 ± 2.1 ns (*42*). The hinge region (G26−W28) is as well-ordered on the picosecond to nanosecond time scale as the helical regions, indicating that the N-terminal helix adopts a preferred orientation.

DISCUSSION

The *Rb. sphaeroides* LH1 β subunit folds as a helix−hinge−helix structure in the detergent micelle system used here. The N-terminal amphipathic helix lies partially embedded in the micelle surface at an approximately 60° angle relative to the C-terminal helix which is inserted into the detergent micelle (Figure 6C). The observed fold is in good agreement with predictions from its sequence (*52*), the distribution of hydrophilic and hydrophobic residues for aligned LH polypeptides (*53*), and the β subunit structure determined in organic solvents (*15*). The overall helicity of the β subunit structure reported here is 65%, in good agreement with far-UV CD data (*16*, *54*, *55*). The structure of the β subunit in the Zwittergent 3:12 micelle is of particular interest because it retains the ability to bind BChl *a* and form the B820 subcomplex, unlike the protein in mixed solvents (*15*).

The C-terminal membrane-spanning helix is approximately 25 Å in length with four helical turns. Its overall shape is slightly curved, exposing the conserved H38 for BChl *a* binding. Residues Y42 and R45, which are known to be involved in binding BChl *a* (*49*, *56*−*58*), lie on the same side of the helix as H38. The position of the transmembrane helix in the micelle inferred from NOE and Mn^{2+} relaxation data would place Y23 and W44 at opposite membrane interfaces, a preferential location for aromatic side chains (*59*, *60*). The C-terminus folds back toward the membrane-spanning helix, but does not place the indole side chain of W47 in a position that would hydrogen bond to BChl *a* (*57*, *58*) on the same plane as H38.

The N-terminal helix begins at T12, even though G10 and L11 are conserved in all photosynthetic bacterial species, and extends through S25. It is possible that the N-termius (A1−L11) becomes structured in the presence of the LH1 α subunit and RC components, since there are helical characteristics in this region. In addition, the lack of charged amino acids (L6−L11) suggests the N-terminus should be buried, and this may also occur in the presence of the LH1 α subunit and the RC. The N-terminus forms an amphipathic helix with charges and polar groups on one face (D13, E14, Q15, Q17, and E18) and hydrophobic residues on the other (T12, A16, L19, V22, and Y23). Mn^{2+}-induced relaxation and the detergent NOE patterns showed a helical periodicity in the N-terminal helix. The data presented here support interactions of the charged face with Zwittergent 3:12's charged headgroups and the hydrophobic face with the micelle interior. So, in the Zwittergent 3:12 micelle, the C-terminal helix traverses the core of the micelle, the N-terminal helix lies along the micelle surface, and a hinge is required to connect the two. This observation could explain why Zwittergent 3:12, Zwittergent 3:14, and DPC were the most stable detergents that were tested because they most resemble the native membrane lipid in chain length and charge [phosphatidylethanolamine (40%), phoshphatidylcholine (18%), phosphatidylglycerol (27%), and sulfolipids (3%) (*61*)].

The NMR data presented here support the presence of a hinge region between the transmembrane and surface helices. Only half as many NOEs involving amide protons were observed for residues G26−W28 as were observed for the two helical segments. The hydrogen bonding network stops in the hinge region, consistent with a break in the helical structure. The smallest deviations from random coil carbon chemical shifts in the ordered region of the β subunit are in the hinge region. Relaxation data show that the hinge region is ordered on the picosecond to nanosecond time scale, similar to the two helical regions. This would indicate that the hinge region is not highly flexible. Comparable ^{15}N relaxation data were observed for the major bacteriophage coat protein Ike in MPG micelles, in that a hinge region possesses picosecond to nanosecond dynamics similar to those of the N-terminal amphipathic and C-terminal helices (*62*). However, the observation of weak and broad signals from residues in the hinge region of the β subunit suggests that slower (microsecond to millisecond) motion takes place. Weaker signals were also observed in the area around the hinge region for the Ike protein, and model free analysis

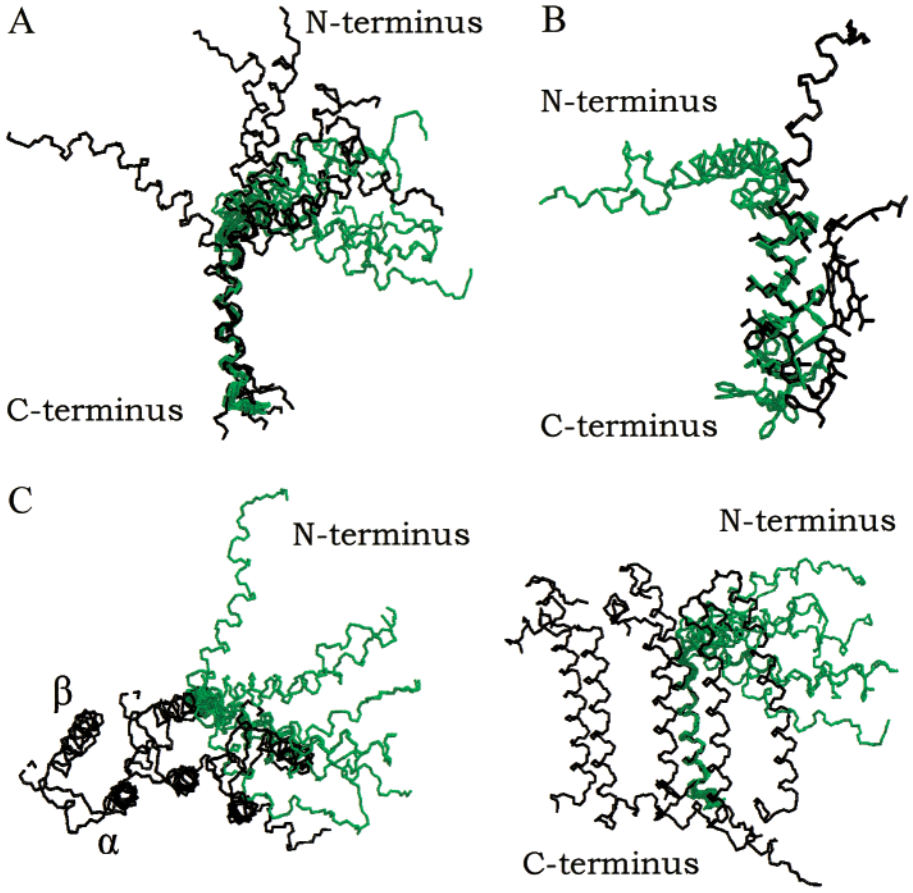

FIGURE 8: Comparison of the *Rb. sphaeroides* LH1 β subunit structures in detergent micelles with (A) the *Rb. sphaeroides* LH1 β subunit in organic solvents and (B) the *Rps. acidophilia* strain 10050 LH2 β subunit with a B850 BChl *a* molecule. (C) Top and side view from a portion of the *Rps. acidophilia* strain 10050 LH2 complex illustrating three outer β subunits and three inner α subunits. The β subunits are aligned with the C-terminal helix from the LH1 β subunit in detergent micelles. The LH1 β subunit in detergent micelles is colored green.

showed slow exchange, suggesting conformational flexibility in the hinge residues (*62*). Though less pronounced, the observation of a hinge in the β subunit in organic solvents provides further support for its importance, since organic solvents have been shown to stabilize and even induce helical conformations (*63*).

A wealth of indirect data also supports the results observed here, with the N-terminal helix partially embedded in the micelle, connected to the transmembrane helix by a hinge. The LH1 β subunit has been shown to be in close contact with the LH1 α subunit and the RC by chemical cross-linking (*64*). This is supported by the modeled projection map of the *Rs. rubrum* LH1 complex by Conroy et al. (*15*), which fits the extra outer mass in the projection map to the N-terminus of the β subunit. Proteolytic studies of the β subunit in the B870 subcomplex showed that much of the N-terminus is protected from digestion. Specific N-terminal amino acids have been shown to be necessary for LH1 formation, as determined by a variety of methods, including protease treatment (*65*), acid hydrolysis (*65*), heterologous reconstitution (*66*), site-specific mutagenesis (*49*), and truncated synthetic peptides (*67*). To explain why an αβ B820 structure is more stable than a ββ B820 structure, Loach et al. (*66*) described possible αβ B820 interactions involving the N-terminus of β which are caused by inter-polypeptide ion pairing, hydrogen bonding capability, and side chain associations. These data suggest that the β subunit folds inward, making specific interactions with the LH1 α subunit and the RC to afford protection.

The LH1 β subunit is one of the first cases of a protein structure being determined in both an organic solvent mixture and a detergent micelle environment. Although the hinge described here differs from the one observed in organic solvents (Figure 8A) (*15*), the overall structures under the two solution conditions are quite similar to each other (Figure 8A). The local rmsds between the best conformer of each family are 0.7 and 0.6 Å for the N- and C-terminal helices, respectively. The C-terminal helices even share the same curvature under both solution conditions. The hinge region for both β subunits is centered at a relatively similar point, W28. On the other hand, the angle adopted by the hinge region and the location of a true break in secondary structure between the N- and C-terminal helices are different between the β subunits. The N-terminal helix lying along the detergent micelle surface adopts a 60° angle with respect to the C-terminal helix, while in organic solvents, the β subunit adopts an approximately 30° angle. This would place the N-terminal helix of the organic solvent β subunit structure fully exposed to the solvent. The location of the break between the N- and C-terminal helices occurs at the hinge region for the detergent β subunit, while the hinge region is calculated to be helical for the β subunit in organic solvents. Therefore, the location for the break for the organic solvent β subunit extends around H20, while for the detergent β

subunit it extends around L27. The accentuated bend in the hinge region for the detergent β subunit is likely a result of interactions between the N-terminal helix and the detergent micelle. The protein also seems to adopt a better defined fold in detergent micelles. Local and overall rmsds and violations of NOE constraints are significantly higher in mixed solvent (*15*), indicating more conformational flexibility or heterogeneity in the absence of a micelle. And, ultimately, it appears that higher-order complexes can only be studied in a micellar environment, since the subunit does not bind BChl *a* in mixed solvents (*15*).

The helix−hinge−helix motif for a small membrane protein is not unique to the LH1 β subunit. The major bacteriophage coat proteins gVIIIp in SDS and DPC micelles, fd in SDS micelles, and Ike in myristoyllysophosphatidylglycerol (MPG) micelles have one hydrophobic helix that spans the micelle, and a second amphipathic helix on the surface of the micelle (*62*, *68*−*70*). One difference between the β subunit and the others is that the depth of the hinge in the micelle places the amphipathic helix for the β subunit more deeply embedded in the membrane than the N-terminal helix of the gVIIIp, fd, and Ike proteins.

Although the structure determined here may be identical to that of the β subunit in the B820 and LH1 complexes, it seems likely that in absence of BChl *a* the C-terminus of the β subunit is in an intermediate conformation between a completely extended conformation and the BChl *a*-bound conformation. This is evident when comparing the C-terminus and C-terminal helix of the organic solvent (Figure 8A) and *Rhodopseudomonas acidophilia* LH2 β subunit structures (Figure 8B,C) (*1*, *15*). The C-terminus of the β subunit in organic solvents is extended and does not fold back toward the C-terminal helix, while the LH2 β subunit folds back toward the C-terminal helix so the indole side chain of W39 is on the same plan as H30 to interact with BChl *a*. The distance between the conserved histidine and tryptophan in both *Rb. sphaeroides* and *Rps. acidophilia* β subunits is nine amino acids which suggests that the two membrane-spanning structures should be similar and, thus, the C-terminus of LH1 β should fold toward H38. This is supported by data showing the *Rhodospirillum molischianum* B850 binding site to be similar to the *Rb. sphaeroides* B875 binding site (*57*, *58*, *71*, *72*).

The backbone of the C-terminal helix of the LH1 β subunit in detergent micelles is similar to that of the subunit in organic solvents and the LH2 β subunit in the intact complex with rmsds of 0.6 and 0.4 Å, respectively. Although there is some overall side chain correlation among the three structures, more divergence occurs between the structures here, as is evident in the side chain of H38. In organic solvents and in LH2, the favored rotamer of the H38 side chain of the β subunit is oriented in a way that would allow for proper interactions with BChl *a* in LH2 (Figure 8B). In only one of the 10 structures calculated in this study was the histidine side chain oriented similarly (Figure 8B). Taken together with the conformation of the C-terminus, the variable side chain conformations suggest that the monomeric β subunit in detergent micelles is likely in a more open conformation favorable for BChl *a* binding. Once the β subunit binds BChl *a*, it would adopt a more closed conformation, with less side chain variability.

Similary, the N-terminus of the β subunit is most likely in an intermediate conformation in the detergent micelle structure. The major differences observed between the structures calculated for the LH1 β subunit are due to the rotation of the N-terminus on the surface of the micelle relative to the C-terminal helix. The angle between the two helices does not change, nor do the interaction surfaces of the N-terminal amphipathic helix with the detergent and solution. The relaxation data support the presence of an ordered hinge region, as reflected in a low rmsd (0.6 Å) for the hinge residues (G26−W28), yet conformational exchange or rotation of the N-terminal helix would explain elevated rmsds compared to those of the C- and N-terminal helices. It would be expected that the conformation of the N-terminal helix becomes fixed in the presence of the other LH1 components, so this observation again suggests that the protein is in an intermediate conformation that is favorable for BChl *a* and α subunit binding.

The major difference between the β subunit in LH1 and LH2 appears to be simply the orientation of the N-terminal helix, which extends into the solvent in the LH2 structure. It will be interesting to investigate the LH1 β subunit in the presence of the LH1 α subunit and BChl *a* to discern what structural differences cause the large observed functional differences between the two complexes. These include the number of bound BChl *a*, the optical absorbance spectrum, the ring size and stability, and interactions with the RC. A structure of the B820 subcomplex will aid our understanding of LH1 light harvesting and energy transfer to the RC.

REFERENCES

1. McDermott, G., Prince, S. M., Freer, A. A., Hawthornthwaite-Lawless, A. M., Papiz, M. Z., Cogdell, R. J., and Isaacs, N. W. (1995) *Nature 374*, 517−521.
2. Koepke, J., Hu, X., Muenke, C., Schulten, K., and Michel, H. (1996) *Structure 4*, 581−597.
3. Deisenhofer, J., Epp, O., Miki, K., Huber, R., and Michel, H. (1985) *Nature 318*, 618−624.
4. Allen, J. P., Feher, G., Yeates, T. O., Rees, D. C., Deisenhofer, J., and Michel, H., and Huber, R. (1986) *Proc. Natl. Acad. Sci. U.S.A. 83*, 8589−8593.
5. Xia, D., Yu, C. A., Kim, H., Xia, J. Z., Kachurin, A. M., Zhang, L., Yu, L., and Deisenhofer, J. (1997) *Science 277*, 60−66.
6. Karrasch, S., Bullough, P. A., and Gosh, R. (1995) *EMBO J. 14*, 631−638.
7. Sauer, K., and Austin, L. A. (1978) *Biochemistry 17*, 2011−2019.
8. Broglie, R. M., Hunter, C. N., Delepelaire, P., Niederman, R. A., Chua, N. H., and Clayton, R. K. (1980) *Proc. Natl. Acad. Sci. U.S.A. 77*, 87−91.
9. Cogdell, R. J., Lindsay, J. G., Valentine, J., and Durant, I. (1982) *FEBS Lett. 150*, 151−154.
10. Picorel, R., Belanger, G., and Gingras, G. (1983) *Biochemistry 22*, 2491−2497.
11. Walz, T., and Ghosh, R. (1997) *J. Mol. Biol. 265*, 107−111.
12. Walz, T., Jamieson, S. J., Bowers, C. M., Bullough, P. A., and Hunter, C. N. (1998) *J. Mol. Biol. 282*, 833−845.
13. Hu, X., Damjanovic, A., Ritz, T., and Schulten, K. (1998) *Proc. Natl. Acad. Sci. U.S.A. 95*, 5935−5941.
14. Hu, X., and Schulten, K. (1998) *Biophys. J. 75*, 683−694.
15. Conroy, M. J., Westerhuis, W. H., Parkes-Loach, P. S., Loach, P. A., Hunter, C. N., and Williamson, M. P. (2000) *J. Mol. Biol. 298*, 83−94.
16. Ghosh, R., Hauser, H., and Bachofen, R. (1988) *Biochemistry 27*, 1004−1014.
17. Davis, C. M., Bustamante, P. L., and Loach, P. A. (1995) *J. Biol. Chem. 270*, 5793−5804.

18. Tadros, M. H., Suter, F., Seydewitz, H. H., Witt, I., Zuber, H., and Drews, G. (1984) *Eur. J. Biochem. 138*, 209−212.
19. Scheer, H. (1991) *Chlorophylls*, CRC Press, Boca Raton, FL.
20. Bax, A., and Pochapsky, S. S. (1992) *J. Magn. Reson. 99*, 638.
21. Kay, L. E., Keifer, P., and Saarinen, T. (1992) *J. Am. Chem. Soc. 114*, 10663.
22. Palmer, A. G., Cavanagh, J., Wright, P. E., and Rance, M. (1991) *J. Magn. Reson. 93*, 151.
23. Marion, D., Ikura, M., Tschudin, R., and Bax, A. (1989) *J. Magn. Reson. 85*, 393.
24. Wishart, D. S., Bigam, C. G., Yao, J., Abildgaard, F., Dyson, H. J., Oldfield, E., Markley, J. L., and Sykes, B. D. (1995) *J. Biomol. NMR 6*, 135−140.
25. Delaglio, F., Grzesiek, S., Vuister, G. W., Zhu, G., Pfeifer, J., and Bax, A. (1995) *J. Biomol. NMR 6*, 689−707.
26. Johnson, B. A., and Blevins, R. A. (1994) *J. Biol. Phys. 29*, 1012−1014.
27. Wittekind, M., and Mueller, L. (1993) *J. Magn. Reson., Ser. B 101*, 201−205.
28. Grzesiek, S., and Bax, A. (1992) *J. Am. Chem. Soc. 114*, 6291−6293.
29. Kay, L. E., Ikura, M., Tschudin, R., and Bax, J. (1990) *J. Magn. Reson. 89*, 496−514.
30. Grzesiek, S., and Bax, A. (1992) *J. Magn. Reson. 96*, 432−440.
31. Grzesiek, S., Anglister, J., and Bax, A. (1993) *J. Magn. Reson., Ser. B 101*, 114−119.
32. Vuister, G. W., and Bax, A. (1993) *J. Am. Chem. Soc. 115*, 7772−7777.
33. Powers, R., Gronenborn, A. M., Clore, G. M., and Bax, A. (1991) *J. Magn. Reson. 94*, 209−213.
34. Kay, L. E., Xu, G. Y., Singer, A. U., Muhandiram, R., and Forman-Kay, J. D. (1993) *J. Magn. Reson., Ser. B 101*, 333.
35. Zhang, O., Kay, L. E., Olivier, J. P., and Forman-Kay, J. D. (1994) *J. Biomol. NMR 4*, 845.
36. Czerski, L., Vinogradova, O., and Sanders, C. R. (2000) *J. Magn. Reson. 142*, 111−119.
37. Baxter, N. J., and Williamson, M. P. (1997) *J. Biomol. NMR. 9*, 359−369.
38. Skelton, N. J., Palmer, A. G. I., Akke, M., Kordel, J., Rance, M., and Chazin, W. J. (1993) *J. Magn. Reson., Ser. B 102*, 253−264.
39. Piotto, M., Saudek, M., and Sklenar, V. (1992) *J. Biomol. NMR 2*, 661−665.
40. Fushman, D., Cahill, S., and Cowburn, D. (1997) *J. Mol. Biol. 266*, 173−194.
41. Grzesiek, S., and Bax, A. (1993) *J. Am. Chem. Soc. 115*, 12593−12594.
42. Orekhov, V. Y., Nolde, D. E., Golovanov, A. P., Korzhnev, D. M., and Arseniev, A. S. (1995) *Appl. Magn. Reson. 9*, 581−588.
43. Brunger, A. T., Adams, P. D., Clore, G. M., DeLano, W. L., Gros, P., Grosse-Kunstleve, R. W., Jiang, J. S., Kuszewski, J., Nilges, M., Pannu, N. S., Read, R. J., Rice, L. M., Simonson, T., and Warren, G. L. (1998) *Acta Crystallogr. D54*, 905−921.
44. Cornilescu, G., Delaglio, F., and Bax, A. (1999) *J. Biomol. NMR 13*, 289−302.
45. Laskowski, R. A., Rullmann, J. A. C., MacArthur, M. W., Kaptein, R., and Thornton, J. M. (1996) *J. Biomol. NMR 8*, 477.
46. Parkes-Loach, P. S., Sprinkle, J. R., and Loach, P. A. (1988) *Biochemistry 27*, 2718−2727.
47. Chang, M. C., Callahan, P. M., Parkes-Loach, P. S., Cotton, T. M., and Loach, P. A. (1990) *Biochemistry 29*, 421−429.
48. Sturgis, J. N., and Robert, B. (1994) *J. Mol. Biol. 238*, 445−454.
49. Davis, C. M., Bustamante, P. L., Todd, J. B., Parkes-Loach, P. S., McGlynn, P., Olsen, J. D., McMaster, L., Hunter, C. N., and Loach, P. A. (1997) *Biochemistry 36*, 3671−3679.
50. Byers, S., Hopkins, T. J., Kuettner, K. E., and Kimura, J. H. (1987) *J. Biol. Chem. 262*, 9166−9174.
51. Wishart, D. S., Sykes, B. D., and Richards, F. M. (1991) *J. Mol. Biol. 222*, 311−333.
52. Olsen, J. D., and Hunter, C. N. (1994) *Photochem. Photobiol. 60*, 521−535.
53. Donnelly, D., and Cogdell, R. J. (1993) *Protein Eng. 6*, 629−635.
54. Cogdell, R. J., and Scheer, H. (1985) *Photochem. Photobiol. 42*, 669−678.
55. Breton, J., and Nabedryk, E. (1987) in *The Light Reactions* (Barber, J., Ed.) Elsevier, Amsterdam, pp 159−195.
56. Kehoe, J. W., Meadows, K. A., Parkes-Loach, P. S., and Loach, P. A. (1998) *Biochemistry 37*, 3418−3428.
57. Olsen, J. D., Sturgis, J. N., Westerhuis, W. H., Fowler, G. J., Hunter, C. N., and Robert, B. (1997) *Biochemistry 36*, 12625−12632.
58. Sturgis, J. N., Olsen, J. D., Robert, B., and Robert, B. J (1997) *Biochemistry 36*, 2772−2778.
59. Schiffer, M., Chang, C. H., and Stevens, F. J. (1992) *Protein Eng. 5*, 213−214.
60. Cowan, S. W., Schirmer, T., Rummel, G., Steiert, M., Ghosh, R., Pauptit, R. A., Jansonius, J. N., and Rosenbusch, J. P. (1992) *Nature 358*, 727−733.
61. Arondel, V., Benning, C., and Somerville, C. R. (1993) *J. Biol. Chem. 268*, 16002−16008.
62. Williams, K. A., Farrow, N. A., Deber, C. M., and Kay, L. E. (1996) *Biochemistry 35*, 5145−5157.
63. Hirota, N., Mizuno, K., and Goto, Y. (1998) *J. Mol. Biol. 275*, 365−378.
64. Peters, J., Takemoto, J., and Drews, G. (1983) *Biochemistry 22*, 5660−5667.
65. Meadows, K. A., Iida, K., Tsuda, K., Recchia, P. A., Heller, B. A., Antonio, B., Nango, M., and Loach, P. A. (1995) *Biochemistry 34*, 1559−1574.
66. Loach, P. A., Parkes-Loach, P. S., Davis, C. M., and Heller, B. A. (1994) *Photosynth. Res. 40*, 231−245.
67. Meadows, K. A., Parkes-Loach, P. S., Kehoe, J. W., and Loach, P. A. (1998) *Biochemistry 37*, 3411−3417.
68. Papavoine, C. H. M., Konings, R. N. H., Hilbers, C. W., and van de Ven, F. J. M. (1994) *Biochemistry 33*, 12990−12997.
69. Papavoine, C. H. M., Aelen, J. M. A., Konings, R. N. H., Hilbers, C. W., and van de Ven, F. J. M. (1995) *Eur. J. Biochem. 232*, 490−500.
70. McDonnell, P. A., Shon, K., Kim, Y., and Opella, S. J. (1993) *J. Mol. Biol. 233*, 447−463.
71. Germeroth, L., Lottspeich, F., Robert, B., and Michel, H. (1993) *Biochemistry 32*, 5615−5621.
72. Visschers, R. W., Germeroth, L., Michel, H., Monshouwer, R., and van Grondelle, R. (1995) *Biochim. Biophys. Acta 1230*, 147−154.
73. Koradi, R., Billeter, M., and Wuthrich, K. (1996) *J. Mol. Graphics 14*, 51.
74. Ferrin, T. E., Huang, C. C., Jarvis, L. E., and Langridge, R. (1988) *J. Mol. Graphics 6*, 13−27.
75. Ferrin, T. E., Huang, C. C., Jarvis, L. E., and Langridge, R. (1988) *J. Mol. Graphics 6*, 36−37.

BI011576J